MATERIALS SCIENCE

Reentrant tensegrity: A three-periodic, chiral, tensegrity structure that is auxetic

Mathias Oster[1], Marcelo A. Dias[2], Timo de Wolff[3], Myfanwy E. Evans[4]*

We present a three-periodic, chiral, tensegrity structure and demonstrate that it is auxetic. Our tensegrity structure is constructed using the chiral symmetry $\mathbf{\Pi}^+$ cylinder packing, transforming cylinders to elastic elements and cylinder contacts to incompressible rods. The resulting structure displays local reentrant geometry at its vertices and is shown to be auxetic when modeled as an equilibrium configuration of spatial constraints subject to a quasi-static deformation. When the structure is subsequently modeled as a lattice material with elastic elements, the auxetic behavior is again confirmed through finite element modeling. The cubic symmetry of the original structure means that the auxetic behavior is observed in both perpendicular directions and is close to isotropic in magnitude. This structure could be the simplest three-dimensional analog to the two-dimensional reentrant honeycomb. This, alongside the chirality of the structure, makes it an interesting design target for multifunctional materials.

INTRODUCTION

The geometric design of material microstructures allows specific material properties to be prescribed through particular motifs and mechanisms. Additive manufacturing has highlighted the potential for designed materials with targeted functionality. Auxetic structures, being those with a negative Poisson's ratio, are an interesting target in the design of metamaterials. An auxetic material is most simply characterized by a perpendicular expansion on stretching the material in a chosen direction. The two-dimensional (2D) reentrant honeycomb pattern is the quintessential example of auxeticity from geometric design (*1*). Theoretically, some understanding and design principles exist for auxetic structures in $\mathbb{R}^2$ in terms of expansiveness and pseudo-triangulations (*2*); however, a three-periodic counterpart is notoriously hard, because the design rules of the 2D case are not easily generalized to the 3D case. The current breadth of examples using a reentrant vertex geometry involves only a limited number of structures (*3*, *4*). Furthermore, many techniques focus on analyzing existing databases of lattices for possible interesting mechanisms (*5*), which is limited by the breadth of existing framework databases. Here, we propose a previously unknown 3D auxetic structure, alongside its construction technique, which has auxetic behavior both as an idealized geometric motif and a simulated elastic material.

We begin with the idea of a tensegrity, a term that comes from the notion of integrity under tension. Originating in the architectural work of Kenneth Snelson and Buckminster Fuller, tensegrity structures use a combination of tension and compression forces to give the illusion of floating rods in space (*6*, *7*). A tensegrity combines strut elements and cable elements. The struts are extendable rigid bars with a prescribed minimum length, which are typically under a compression force. The cables are elements under tension connecting the rigid bars. The combination of these elements and their internal tension maintain the integrity of the structure. Instead of cable elements, elastic elements under tension could also be used to stabilize the structure.

A tensegrity can be describsed mathematically by a set of vertices that fulfill simple distance constraints. Struts prescribe that the vertices can never be closer than given distance but can be arbitrarily far apart. Vertices connected by a cable can be as close together as desired but not farther apart than the length of the cable. In the case of elastic elements rather than cables, a spring energy can be considered along each of the elements. The equilibrium configuration is then the minimization of the spring energy given the distance constraints of the struts. An interesting parallel to the spatial constraints of a tensegrity structure can be made to sphere packings, where the centers of spheres can never be closer than twice the radius, analogous to the strut constraint (*7*). This idea has also been used to explore configurations and stability of periodic sphere packings (*8*).

Similar to the description of sphere packing, symmetric, periodic packing of cylinders in 3D space is a useful technique in the description of crystalline materials. In the description of a crystal structure, the cylinders represent rods of strongly bonded atoms or groups of atoms. For example, the 3D structure of the mineral Garnet was well known for many years, but the subsequent use of cylinder packings provided a more simple description and understanding of the structure (*9*). More recently, cylinder packings have been used in the design and construction of metal-organic frameworks to achieve topologically robust structures (*10*).

Using the invariant axes of the crystallographic space groups allows the enumeration of the simplest and most symmetric cylinder packings (*11*). The restriction to cubic symmetry (which corresponds to a spatially isotropic material), as well as all rods being related to each other by a symmetry of the packing, yields precisely six distinct cylinder packings (*11*). Relaxing the requirement that the cylinders are straight allows the formation of a more general class of curvilinear cylinder packings, obviously with more geometric freedom. The central axes of the curvilinear cylinders are still along the original directions, but the cylinders can curve past, and weave through, their neighbors (*12*, *13*). A particular set of these curvilinear cylinder packing structures were observed to have what was termed a dilatant property, where mutual straightening of the curvilinear cylinders leads to a homothetic expansion of the material (*13*). This structural mechanism can be used to explain the swelling of mammalian

[1]Institut für Mathematik, Technische Universität Berlin, Germany. [2]Institute for Infrastructure and Environment, School of Engineering, The University of Edinburgh, EH9 3FG Scotland, UK. [3]Institut für Analysis und Algebra, AG Algebra, Technische Universität Braunschweig, Universitätsplatz 2, 38106 Braunschweig, Germany. [4]Institut für Mathematik, Universität Potsdam, Germany.
*Corresponding author. Email: evans@uni-potsdam.de

skin cells on prolonged exposure to water, where the cylindrical packing describes the organization of keratin intermediate filaments in the cells (*13*, *14*).

We take here the dilatant Π^+ cylinder packing (*11*), as shown in Fig. 1. It is also referred to as the β-Mn rod packing, as it describes the chemical structure of β-Mn (*15*, *16*). This packing has the chiral space group symmetry $P4_132$, with three distinct cylinder axes along {1,0,0}, {0,1,0}, and {0,0,1}. The Π^+ packing is described by the vectors

$$\left\{\frac{1}{4},0,u\right\}\left\{\frac{3}{4},\frac{1}{2},u\right\}\left\{u,\frac{1}{4},0\right\}\left\{u,\frac{3}{4},\frac{1}{2}\right\}\left\{0,u,\frac{1}{4}\right\}\left\{\frac{1}{2},u,\frac{3}{4}\right\}$$

where u is any real number, and the periodicity gives the parallel cylinders. When the straight cylinders of Π^+ are relaxed to a curvilinear form, the symmetry of the packing drops to the $I4_132$ space group (which is also chiral) and the packing becomes more dense. This curvilinear packing then displays the dilatant property on cooperative straightening of the curved cylinders (*17*). Figure 1 shows the transformation from an expanded structure with straight cylinders in contact to a compacted structure with helical cylinders.

Inspired by the parallel between tensegrities and sphere packings, we construct a tensegrity from the helical Π^+ cylinder packing by reimagining the structure as follows:

1) At all contacts between cylinders, rigid and incompressible bars are placed, connecting the central axes of the cylinders, with a length twice the cylinder radius. They represent the incompressibility of the cylinder at the contact.

2) Thin elastic elements are placed along the central axes of the cylinders in the packing. These elastic elements connect to the incompressible bars passing through the contact points. These elastic elements span the periodic boundary conditions.

3) The final constraint is that the periodicity of the structure remains, which, in this case, means that three orthonormal translation vectors of the same length remain fixed.

What results are a series of rigid rods suspended in space by a periodic web of elastic filaments. This is our periodic tensegrity structure, as shown in Fig. 1.

The topology of the constructed network is known as **bmn**, as described in the Reticular Chemistry Structure Resource database (*18*): This terminology comes from the relation of the structure to the chemical structure of β-Mn. The structure has $I4_132$ space group symmetry, is embedded in a triply periodic unit cell, and has 24 vertices and 36 edges within each cubic unit cell. The vertices are degree 3, and all display the reentrant geometry characteristic of many auxetic materials, including the 2D reentrant honeycomb pattern. We note that there is a degree of freedom in the construction technique: Depending on the level of dilation/compaction of the starting rod packing (such as the two structures given in Fig. 1), we obtain different configurations of the bmn network, with different sized periodic unit cells of our periodic tensegrity. These structures correspond to a variation of the angle of the reentrant vertices. The structure shown in Fig. 1 is one such structure in this family of structures. The reentrant geometry of the vertices is suggestive of auxetic behavior, and it is this hypothesized behavior that we now investigate more deeply.

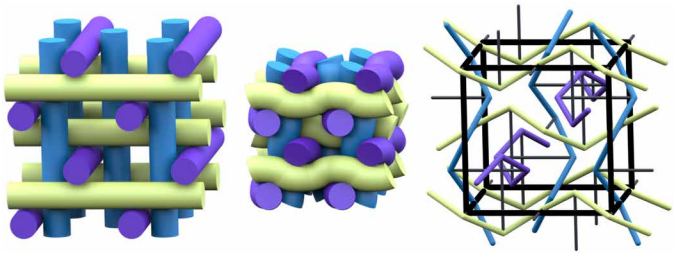

Fig. 1. The Π^+ cylinder packing in three different geometric incarnations. (**Left**) The Π^+ cylinder packing composed of straight cylinders, with chiral space group symmetry $P4_132$, and three distinct cylinder axes. (**Centre**) A compacted version of Π^+ where the cylinders become curvilinear, which now has the chiral space group $I4_132$. (**Right**) The bmn periodic tensegrity structure, where the incompressible rods are shown in black and the elastic struts colored like the cylinder packing above. The periodic unit cell is outlined in the thick black lines.

RESULTS AND DISCUSSION

We investigate the equilibrium configurations and quasi-static deformations of the constructed periodic tensegrity structure. As the starting point for our simulated deformations, we take the configuration shown in Fig. 1, which corresponds to the densest packing of the original cylinder packing, within a fixed unit cell. It can be confirmed numerically by Newton's method that this structure is an equilibrium configuration, where the spring energy is at a minimum not assuming minimal spring lengths. We used several perturbed starting configurations to verify the minimization. The deformation process is then modeled by a quasi-static extension that assumes the springs to have length bounded from below by the configuration computed initially.

The behavior of the structure over an initial phase of deformation is dominated by a breaking of symmetry of the highly symmetric initial structure; all of the symmetries of the structure are lost, leaving just periodicity. On further extension, the structure reaches a more stable behavior, which sees an expansion of the structure in both of the perpendicular directions, indicating auxeticity. Figure 2 shows two configurations of the structure during the deformation process, both the starting equilibrium configuration and the maximally deformed, equilibrium structure. As a result of this process, we can measure the y- and z-direction lattice parameter lengths, as plotted in Fig. 3 (top).

The Poisson's ratio is typically defined only for small strain linear elastic behavior. A more subtle formulation is required when considering highly nonlinear elastic materials over large strain intervals. We used two such formulations to analyze the deformation of the tensegrity structure, the instantaneous Poisson's function and the Poisson's ratio using the log transform true strain (*19*). We can calculate the instantaneous Poisson's ratio in terms of the engineering strain at time step t as follows (*19*)

$$\nu_{xy} = \frac{-e_y}{e_x}$$

where x is the direction of applied strain, y is an orthogonal direction, and e_y and e_x are given by

$$e_y = \frac{(L_y)_t - (L_y)_{t-1}}{(L_y)_{t-1}}$$

$$e_x = \frac{(L_x)_t - (L_x)_{t-1}}{(L_x)_{t-1}}$$

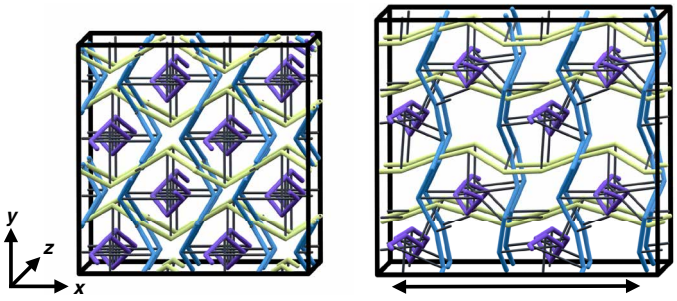

Fig. 2. The geometry of the tensegrity structure under deformation. (**Left**) The starting configuration of our tensegrity structure, shown as a block of $2 \times 2 \times 2$ unit cells. The black cube frame is shown for visualization purposes. The structure is in equilibrium and has the full $I4_132$ symmetry. (**Right**) The structure is stretched along the x axis, and the resulting equilibrium structure is shown. The symmetry of the structure has been broken, for example, the fourfold screwaxes of the helices disappear. The expansion in the perpendicular y direction in response to the stretch can be seen in the size of the deformed structure, and a similar magnitude of expansion is also present in the z direction.

where L_x and L_y are the lattice parameter lengths in the x and y directions taken at time step (t) and the previous time step ($t - 1$). The instantaneous Poisson's function for the deformation of the tensegrity structure is shown in Fig. 3 (middle).

We can also calculate the Poisson's ratio in terms of the log transform true strain at time step t as follows (*19*)

$$\nu_{xy} = -\frac{\eta_y}{\eta_x}$$

where, again, x is the direction of applied strain, y is an orthogonal direction, and η_y and η_x are given by

$$\eta_y = \ln\left(1 + \frac{(L_y)_t - (L_y)_0}{(L_y)_0}\right)$$

$$\eta_x = \ln\left(1 + \frac{(L_x)_t - (L_x)_0}{(L_x)_0}\right)$$

where L_x and L_y are the lattice parameter lengths in the x and y directions taken at time step (t) and the original configuration. The Poisson's ratio calculated using the log transform true strain for the tensegrity structure is shown in Fig. 3 (bottom).

The magnitudes of the instantaneous Poisson's function and the Poisson's ratio using the log transform normal strain are both comparable, as expected from previous results comparing these formulations. The Poisson's ratio is around −1.1 in the y direction and −0.75 in the z direction in the steady state. The cubic symmetry of the structure should imply that the Poisson's ratio is the same in both the y and z directions; however, in this case, the complete loss of symmetry that occurs with the initial deformation results in these directions no longer being equivalent. The choice of which direction gives a larger or smaller Poisson's ratio is also arbitrary and depends of the minimizing configuration found. Despite these differences arising from the symmetry breaking, the auxetic response of the structure stays close to isotropic in the x, y, and z directions, which is a remarkable property for a 3D material.

The phase of deformation directly after the initial loss of symmetry of the structure is highly interesting from both a material science and numerical perspective. It is instructive to explore the stability of these minimizing configurations in more detail; however, the numerical tools are still under development.

We now turn our attention to the engineering potential of realizing these idealized geometric constructions. This is done by extending

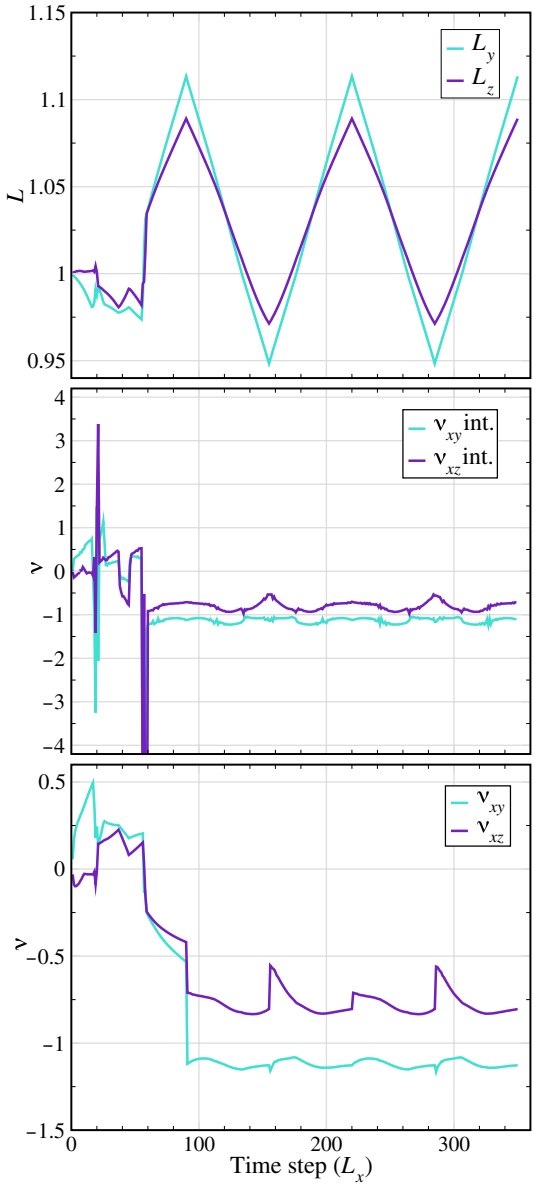

Fig. 3. Measurement of the mechanics of the tensegrity structure under deformation. (**Top**) The length of periodic lattice translation in the y and z directions (L_y and L_z) on repeated extension and compression cycles (cyclical L_x). One can see that, after an initial phase of instability, the structure reaches a steady state of expansion in the y and z directions during expansion in the x direction and, likewise, contraction when x is contracted. (**Middle**) The instantaneous Poisson's function (ν_{xy} and ν_{xz}) on repeated extension and compression cycles of the structure in the x direction. The values reach a relatively steady state of around −1.1 for ν_{xy} and − 0.75 for ν_{xz}. (**Bottom**) The Poisson's ratio (ν_{xy} and ν_{xz}) computed using the log transform true strain on repeated extension and compression cycles of the structure in the x direction. The values reached here are comparable to those seen in the instantaneous Poisson's function above.

the concept of the auxetic periodic tensegrity structures to finite 3D lattices composed of elastic elements. For such more realistic situations, the driving principle toward auxeticity depends on the interplay between geometry and elasticity (*20*, *21*)—by turning a mechanism into an actual structure, through locking of the hinge points, loading carrying will occur via axial stresses and bending moments.

The boundary conditions were enforced constraining the normal displacements of the elements for the lattice's planes at $x = 0$, $y = 0$, and $z = 0$. A quasi-static and displacement controlled condition was applied to the end of the cable elements at the plane $x = n \times L$ (where L is the length of the unit cell), thus imposing a stretch in the direction normal to the yz plane. First, from Fig. 4, we look at the level of axial stresses σ_{11} in each element. As expected, from a tensegrity structure, tension and compression will be carried by the cables and struts, respectively. By zooming in to a representative volume in the interior of the lattice, as shown in Fig. 4, we noticed that $\sigma_{11} > 0$ for the "cable" elements and $\sigma_{11} < 0$ for the struts. We further measure the effective structural Poisson's ratio, as shown in Fig. 5, and we observe that ν_{xy} and ν_{xz} depend in a nonmonotonic manner with respect to the diameter ratio d_c/d_s, which is here seen as a design parameter. Notice that auxeticity can be maximized for $1 \lesssim d_c/d_s \lesssim 1.6$, depending on the direction of the deformation. In Fig. 6, we show two perspectives, xy and xz, of center unit cells in $8 \times 8 \times 8$ lattices, in their rest and deformed configurations. To highlight the effect of curvature on each of the elements, we show two examples of aspect ratios $d_c/d_s = 0.6$ and $d_c/d_s = 1.2$, coloring the elements by the absolute value of the total curvature vector $\boldsymbol{\kappa}$—here, its components in the moving frame parameterized by the arc length are two normal curvatures and one twist. Notice that the effect of auxeticity is derived from the fact that there is a local increase of voids' size within the unit cell, which is the same phenomenon observed in the idealized mechanism seen in Fig. 2. However, given that, in the real structure where the hinges are locked, the moment balance at the nodes leads to an increase in the curvature of the cable elements, which results in less "free length" for the expansion in all directions. Hence, the difference in the Poisson's ratio observed in Fig. 5 against the values $\nu_{xy} = -1.1$ and $\nu_{xz} = -0.75$ is computed for the idealized case, as shown in Fig. 2. We choose to demonstrate this effect from the curvature data because it gives us an intuitive geometric measure of the causal relationship between curvatures and the moments transferred by the joints via the bending rigidity of the element, i.e., the constitutive behavior of the elements.

To further extend these ideas to real materials, we explored 3D printing of a toy model of the structure. We printed in a single material, using rubber-like thermoplastic polyurethane, without differentiating between the rigid and elastic elements. The radius of the rigid and elastic in the printed is the same, which would correspond to the case of $d_c/d_s = 1$ in the simulations. Despite this simplification, we were able to observe mild auxetic behavior of the structure (Fig. 7). A full movie of the deformation is included in the Supplementary Materials.

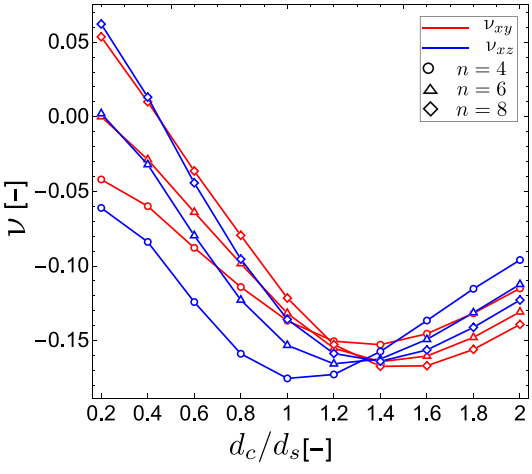

Fig. 5. Poisson's ratio of the structure. It shows the Poisson's ratio ν_{xy} and ν_{xz}, as a function of the diameter ratio d_c/d_s between the of the cable and the strut elements. The results for lattice assemblies with different numbers of unit cells, n, are shown.

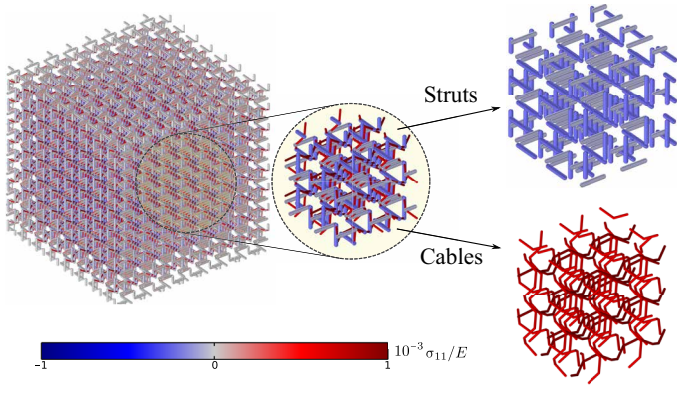

Fig. 4. Tension and compression of the tensegrity elements. $8 \times 8 \times 8$ lattice for $d_c/d_s = 0.6$. The color map represents the level of axial stresses σ_{11}, normalized by the Young's modulus E, along the elements' arc lengths. The inset shows a representative volume and further the dissection of the cable and the strut elements to show that they are subjected to tension and compression, respectively. The deformed configurations are shown at 0.025 strain.

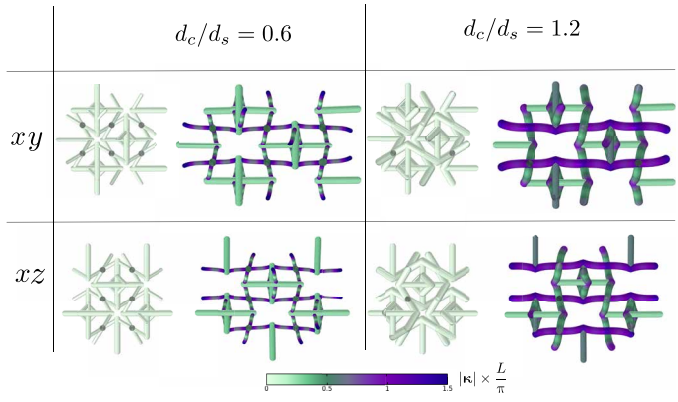

Fig. 6. The effect of curvature on each of the elements. Unit cell's rest and deformed configurations for $d_c/d_s = 0.6$ and $d_c/d_s = 1.2$ from a $8 \times 8 \times 8$ lattice. The color map represents the norm of the curvature vector $\boldsymbol{\kappa}$. Two different perspectives are presented, xy and xz. The deformed configurations are shown at 0.75 strain.

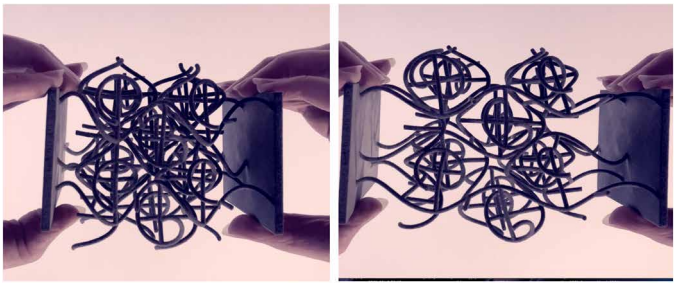

Fig. 7. Deformation of a 3D print of a block of the tensegrity structure. The object is printed using rubber-like thermoplastic polyurethane material. The full structure is printed in the same material, so there is no differentiation made between the incompressible bars and the elastic elements. Despite this highly simplified design, we still observe auxetic behavior.

In summary, we have described here a method for constructing a chiral, triply periodic tensegrity structure, based on the high symmetry Π^+ rod packing, well known from structural chemistry. It displays local reentrant geometry at all of its vertices, giving the structure an auxetic behavior on quasi-static extension and compression deformations. We have demonstrated that this auxetic behavior also carries over the realistic material simulation. The quantitative differences in the values of ν_{xy} and ν_{xz}, contrasting the computations for the idealized structure and that which is obtained from finite element method (FEM), are attributed to the overconstrained hinges in the more realistic situation—this is seen by the gain in curvature of the elements at a cost of free length, as shown in Fig. 6. The structure presented here is potentially the simplest three-periodic incarnation of the reentrant honeycomb motif and, as such, is an interesting design target for framework materials. In particular, the relationship of the tensegrity structure to the original rod packing suggests that this could be an interesting design target in the metal-organic framework context, where rod packings are already realistic design targets. Given that the structure is also chiral, this suggests that the structure could be a target for metamaterials, where chirality is a precursor to an array of functionality in materials, particularly electrical, optical, and magnetic properties.

The auxetic behavior is related to the original dilatant property of the Π^+ rod packing. There are a suite of similar curvilinear cylinder packings described in (*13*), all displaying the dilatant property, and we expect that the conversion of these packings to tensegrity structures using the methodology described here should lead to similar auxetic behavior. In particular, the Σ^+ cylinder packing that appears in the microstructure of mammalian skin cells displays a particularly large degree of dilatancy, and we expect it to be an interesting target material (*14*). This process of using dilatant rod packings as a construction technique for auxetic tensegrity structures opens a design technique for a wide array of auxetic materials, which inherit the low-density characteristics of the original cylinder packings.

The analysis of this structure instigated various explorations in available tools from the fields of algebraic geometry and optimization. It was apparent in most situations that the structure was too complicated for most of the available numerical tools, although from a materials science perspective, the tensegrity structure is relatively simple. This has already prompted the development of new numerical and symbolical approaches in these fields of mathematics (*22*–*24*), and we are optimistic about the use of these tools in further studies of this type.

MATERIALS AND METHODS

We investigated the equilibrium configurations and quasi-static deformations of the constructed periodic tensegrity structure. For any of our constructed tensegrity structures with different degrees of compression, we calculated the equilibrium configuration (*6*). If we place springs along each of the elastic cables, then these will each have an energy proportional to the square of their length. If we minimize this collectively while maintaining all of the length conditions of the tensegrity, then the equilibrium configuration can be found. The periodicity of the structure for a fixed unit cell size is incorporated through additional constraints keeping vertices related to copies of themselves by the orthonormal periodicity vectors. Noticing that the discrete Laplacian (*25*) fulfills Hooke's law at each vertex of the structure, we interpret the spring energy of the tensegrity as the discrete Dirichlet energy $\mathcal{E}$ on the vertex set V and edge set E of the unit cell. Using this idea, one gets

$$\frac{\partial}{\partial f_i}\mathcal{E}(f) = \frac{\partial}{\partial f_i}\left(\frac{1}{2}\sum_{ij\in E}\mu_{ij}\|f_i - f_j\|^2\right) = \sum_{j:ij\in E}\mu_{ij}(f_i - f_j)$$

where $ij \in E$ is an edge between vertices i and j, and $j : ij \in E$ are all vertices j that share an edge with vertex i. Furthermore, $\mu_{ij} > 0$ is the spring constant, $\|\cdot\|$ denotes the Euclidean norm, and $f: V \to \mathbb{R}^3$ is a realization of the network, i.e., f_i are the Euclidean coordinates of a vertex i for the actual configuration.

As an alternative approach, we can interpret the incompressible bars as springs with fixed lengths and assume a momenta and torque-free equilibrium, and the following optimization problem arises

$$\min_{f:V\to\mathbb{R}^3}\frac{1}{2}\sum_{ij\in E}\|f_i - f_j\|^2$$

under the constraints

1) $\|f_i - f_j\|^2 =$ length (bars) = constant if ij is an incompressible bar
2) $\|f_i - f_j\|^2 \geq l_{ij}^{\min}$ if ij is a spring of minimal length $l_{ij}^{\min}$
3) $\sum$torque $= \sum_{j:ij\in E}(f_i \times (f_i - f_j)) = 0$

where $\times$ denotes the cross product in three dimensions. This amounts to a polynomial optimization problem over semialgebraic sets. However, the number of variables in the problem is too high for the usual sums of squares/semidefinite programming–based approach in polynomial optimization [implemented in the packages like GloptiPoly (*26*)], resulting in memory overflow. Thus, we used the solvers of constrained optimization preimplemented in MATLAB. These solvers cannot guarantee to find a globally optimal solution; however, they will find local equilibrium configurations. MATLAB provides multiple solvers (*27*) that give consistent results for our problem. Here, we use the results obtained by the interior point algorithm (*28*), which replaces the inequality constraints by a sequence of equality constrained minimization problems involving logarithmic barrier functions that are solved either by Newton's method or conjugate gradient steps.

We perform the quasi-static extension (and then subsequent compression) of the structure with small step sizes (0.0025) by changing the lattice parameter length of the structure in one direction (in this

case, the x direction) while observing how the structure reacts to this deformation and finds a new equilibirum. The lattice parameter lengths perpendicular to the deformation direction (in this case, y and z directions) are free variables in the optimization process. At this point, it is important to consider a minimal spring length to avoid collapse of the structure. The cubic symmetry of the structure ensures the generality of choosing a single deformation direction.

In the context of the 3D material consisting of elastic elements, we apply the FEM to 3D lattice assemblies of $n \times n \times n$ bmn unit cells, shown in Fig. 1, where n is an integer number that assigns the number of unit cells. The FEM simulations were performed in the commercial software COMSOL Multiphysics. The elastic elements are modeled as intrinsically 1D variational problems, i.e., using line elements for an Euler-Bernoulli beam formulation. This implies that the elastic elements, in contrast with the idealized strut elements and cable elements, are all subjected to line tensions and bending moments. We assume that the cross sections of the elastic elements are circular, where the strut elements have diameter d_s and cable elements d_c. A Hookean rubber-like material is chosen, where the Young's modulus is $E = 0.1$ GPa and Poisson's ratio $\nu = 0.49$—because auxeticity is dominated by geometry, the choice of base material does not play a key role in our discussion. We searched for solutions with the default stationary solver, where Newton's method is implemented. Mesh refinement studies were undertaken to ensure convergence of the results.

SUPPLEMENTARY MATERIALS

Supplementary material for this article is available at https://science.org/doi/10.1126/sciadv.abj6737

REFERENCES AND NOTES

1. R. S. Lakes, Response: Negative poisson's ratio materials. *Science* **238**, 551 (1987).
2. C. S. Borcea, I. Streinu, Geometric auxetics. *Proc. R. Soc. A* **471**, 20150033 (2015).
3. R. F. Almgren, An isotropic three-dimensional structure with Poisson's ratio = − 1. *J. Elast.* **15**, 427–430 (1985).
4. T. Bückmann, N. Stenger, M. Kadic, J. Kaschke, A. Frölich, T. Kennerknecht, C. Eberl, M. Thiel, M. Wegener, Tailored 3d mechanical metamaterials made by dip-in direct-laser-writing optical lithography. *Adv. Mater.* **24**, 2710–2714 (2012).
5. C. Körner, Y. Liebold-Ribeiro, A systematic approach to identify cellular auxetic materials. *Smart Mater. Struct.* **24**, 025013 (2015).
6. B. Roth, W. Whiteley, Tensegrity frameworks. *Trans. Am. Math. Soc.* **265**, 419–446 (1981).
7. R. Connelly, A. Back, Mathematics and tensegrity. *Am. Sci.* **86**, 142–151 (1998).
8. R. Connelly, J. D. Shen, A. D. Smith, Ball packings with periodic constraints. *Discrete Comput. Geom.* **52**, 754–779 (2014).
9. S. Andersson, M. O'Keeffe, Body-centred cubic cylinder packing and the garnet structure. *Nature* **267**, 605–606 (1977).
10. N. L. Rosi, J. Kim, M. Eddaoudi, B. Chen, M. O'Keeffe, O. M. Yaghi, Rod packings and metal-organic frameworks constructed from rod-shaped secondary building units. *J. Am. Chem. Soc.* **127**, 1504–1518 (2005).
11. M. O'Keeffe, J. Plevert, Y. Teshima, Y. Watanabe, T. Ogama, The invariant cubic rod (cylinder) packings: Symmetries and coordinates. *Acta Crystallogr. A* **57**, 110–111 (2001).
12. M. E. Evans, V. Robins, S. T. Hyde, Periodic entanglement II: Weavings from hyperbolic line patterns. *Acta Crystallogr. A* **69**, 262–275 (2013).
13. M. E. Evans, S. T. Hyde, From three-dimensional weavings to swollen corneocytes. *J. R. Soc. Interface* **8**, 1274–1280 (2011).
14. M. E. Evans, R. Roth, Shaping the skin: The interplay of mesoscale geometry and corneocyte swelling. *Phys. Rev. Lett.* **112**, 038102 (2014).
15. H. Nyman, C. E. Carroll, B. G. Hyde, Rectilinear rods of face-sharing tetrahedra and the structure on β-mn. *Z. Krist.* **196**, 39–46 (1991).
16. S. Lidin, S. Andersson, Regular polyhedra helices. *Z. Anorg. Allg. Chem.* **622**, 164–166 (1996).
17. M. E. Evans, V. Robins, S. T. Hyde, Ideal geometry of periodic entanglements. *Proc. R. Soc. A* **471**, 20150254 (2015).
18. M. O'Keeffe, M. A. Peskov, S. J. Ramsden, O. M. Yaghi, The reticular chemistry structure resource (RCSR) database of, and symbols for, crystal nets. *Accts Chem Res* **41**, 1782–1789 (2008).
19. C. W. Smith, R. J. Wootton, K. E. Evans, Interpretation of experimental data for poisson's ratio of highly nonlinear materials. *Exp. Mech.* **39**, 356–362 (1999).
20. D. J. Rayneau-Kirkhope, M. A. Dias, Recipes for selecting failure modes in 2-d lattices. *Extreme Mech. Lett.* **9**, 11–20 (2016).
21. D. J. Rayneau-Kirkhope, C. Zhang, L. Theran, M. A. Dias, Analytic analysis of auxetic metamaterials through analogy with rigid link systems. *Proc. R. Soc. A* **474**, 20170753 (2018).
22. A. Heaton, S. Timme, Catastrophe in elastic tensegrity frameworks (2020); arXiv:2009.13408.
23. H. P. Le, M. Safey El Din, T. de Wolff, *ISSAC '20: International Symposium on Symbolic and Algebraic Computation, Kalamata, Greece, July 20–23, 2020*, I. Z. Emiris, L. Zhi, Eds. (ACM, 2020), pp. 297–304.
24. H. P. Le, M. Safey El Din, Solving parametric systems of polynomial equations over the reals through hermite matrices (2020); arXiv:2011.14136.
25. A. I. Bobenko, B. A. Springborn, A discrete laplace-beltrami operator for simplicial surfaces. *Discrete Comput. Geom.* **38**, 740–756 (2007).
26. D. Henrion, J.-B. Lasserre, J. Löfberg, Gloptipoly 3: Moments, optimization and semidefinite programming. *Optim. Methods Softw.* **24**, 761–779 (2009).
27. *MATLAB and Optimization Toolbox* (The MathWorks, Inc, 2018).
28. R. Byrd, M. Hribar, J. Nocedal, An interior point algorithm for large-scale nonlinear programming. *SIAM J. Optim.* **9**, 877–900 (1999).

Acknowledgments

Funding: M.E.E. and T.d.W. thank the DFG Emmy Noether Program for support. M.E.E. and T.d.W. were supported by the projects EV 210/1-1 and WO 2206/1-1, respectively. M.E.E. also thanks the DFG Cluster of Excellence "Matters of Activity" for support. **Author contributions:** M.E.E., M.A.D., and T.d.W. designed the research. M.O., M.A.D., and M.E.E. performed the research. M.O., M.A.D., T.d.W., and M.E.E. analyzed the methodologies and results. M.A.D. and M.E.E. wrote the paper. **Competing interests:** The authors declare that they have no competing interests. **Data and materials availability:** All data needed to evaluate the conclusions in the paper are present in the paper and/or the Supplementary Materials.

Submitted 25 May 2021
Accepted 22 October 2021
Published 10 December 2021
10.1126/sciadv.abj6737